Journal of Inorganic and General Chemistry
ZAAC
Zeitschrift für anorganische und allgemeine Chemie
www.zaac.wiley-vch.de
RESEARCH ARTICLE

DOI: 10.1002/zaac.202300244

Special Collection

Synthesis, Crystal structure, electronic structure, and Raman spectra of $Li_4Sr_2SiP_4$

Vincent Daiber,[a] Sabine Zeitz,[a] Viktor Hlukhyy,[a] Dominik Dankert,[a] and Thomas F. Fässler*[a]

Dedicated to Professor Rhett Kempe on the occasion of his 60th birthday.

Recently, ternary lithium phosphides have been studied intensively owing to their high lithium ion conductivities. During investigations aiming for derivatives with less lithium content the new compound $Li_4Sr_2SiP_4$ was obtained. It crystallizes in the monoclinic space group $P2_1/m$ (N°11) with lattice parameters of $a = 7.2919(8)$ Å, $b = 8.3679(6)$ Å, $c = 6.9965(8)$ Å, and $\beta = 90.061(9)°$. The crystal structure contains isolated $[SiP_4]^{8-}$ tetrahedra that are charge balanced by two Sr^{2+} and four Li^+ counter ions. The structure can be derived as a superstructure of the layered $CaAl_2Si_2$ structure type comprising a hexagonal closest packing of P atoms and tetrahedral voids filled with Si and Li atoms, whereas octahedral voids are filled with Sr and Li atoms. DFT calculations confirm the structure with ordered atom positions as a global minimum and predict an indirect band gap of 2.23 eV. In addition, the experimental Raman spectrum is in good agreement with the calculated one.

Introduction

With industry's and society's ever increasing demand for electricity, research on its storage has grown into a widespread field. Among all the technologies invented and improved throughout the last decades, lithium ion batteries play a major role in modern energy storage – either in mobile electrical devices or power source in electrical vehicles. All solid state batteries are hailed as next generation battery technology and hold promise to improve lithium ion batteries even further, especially in terms of safety and energy density.[1]

With Li_8SiP_4,[2] Li_9AlP_4[3] and $Li_{14}TtP_6$ (Tt = Si, Ge, Sn)[4] well performing solid state ionic conductors comprising isolated SiP_4 and AlP_4 tetrahedral units have been presented. The tetrahedra are separated by Li ions and the respective compounds serve as model systems to understand structure property relationships in lithium ion conductors. While isolated SiP_4 tetrahedra are also a known feature of compounds like Sr_4SiP_4,[5] most other members of the phosphido silicate family exhibit different structural motives. Condensed polyhedra can form one-dimensional chains as in K_2SiP_2,[6] two-dimensional layers as in $Ca_2Si_2P_4$[7] or three-dimensional networks as in Li_2SiP_2,[2,8] Li_2SiP_3,[8] KSi_2P_3[9] or $SrSi_7P_{10}$.[10] Furthermore, more complex phosphidosilicates have been reported. They exhibit motifs ranging from Si_4P_5 cages as in $Ba_3Si_4P_6$[11] to SiP_4 tetrahedra linked to each other *via* P–P bonds as in Ea_2SiP_4[12,13] (Ea = Sr, Ba, Eu) or connected by P–P bonds as well as shared vertices and/or corners as in $Ba_4Si_3P_8$[12] or $LaSiP_3$.[14] In this work, we describe follow up research on the possibility of reduction of the lithium content by partial substitution of lithium by alkaline-earth metals. During the investigating of the series $Li_{8-2x}Sr_xSiP_4$ we found the new *Zintl* phase $Li_4Sr_2SiP_4$ ($x = 2$). The compound is structurally closely related to the $CaAl_2Si_2$ structure type,[15] consisting of a hexagonal closest packing (*hcp*) of phosphorous atoms in contrast to the cubic closest packing (*ccp*) observed in Li_8SiP_4. $Li_4Sr_2SiP_4$ crystallizes in a new structure type, linking the $CaAl_2Si_2$ and Li_3LaSb_2 structure type[16] in terms of the occupation of voids by cations.

Experimental Section

Synthesis of $Li_4Sr_2SiP_4$. Li (rods, Rockwood Lithium, 99%) and red P (powder, Sigma Aldrich, 97%) were used without further purification, Sr (pieces, ChemPur, 98%) was mechanically cleaned from oxide surface impurities. Si pieces (Wacker, 99.9%) were ball milled to a fine powder prior to use. Li and Sr were cut into small pieces of approx. 5 mm in diameter to ensure homogeneous distribution during synthesis. $Li_4Sr_2SiP_4$ can be synthesized from stochiometric amounts of the elements either *via* ball milling and subsequent annealing or direct melting of the elements. Direct melting of the elements yields crystals suitable for single crystal analysis as well as side phases while the ball milling route yields the phase pure compound as a polycrystalline powder.

For the ball milling route a reactive mixture was produced by ball-milling for 18 hours at 350 rpm in a 50 mL tungsten carbide (WC)

[a] V. Daiber, S. Zeitz, V. Hlukhyy, D. Dankert, T. F. Fässler
TUM School of Natural Science, Department of Chemistry, Chair of Inorganic Chemistry with Focus on New Materials, Technische Universität München, Lichtenbergstraße 4, D-85747 Garching, Germany
E-mail: thomas.faessler@lrz.tum.de

Supporting information for this article is available on the WWW under https://doi.org/10.1002/zaac.202300244

This article is part of a Special Collection dedicated to Professor Rhett Kempe on the occasion of his 60th birthday. Please see our homepage for more articles in the collection.

jar with 3 WC balls of 15 mm diameter each in a Retch PM 100 planetary mill. The obtained powder was pressed into pellets of ca. 500 mg mass and a diameter of 8 mm under a pressure of 5 tons for a few minutes, resulting in pellets of 2 to 3 mm height. These pellets were sealed in Nb ampoules by arc welding (Edmund Bühler MAM1). The ampoules were transferred in evacuated quartz glass tubes, and placed in a tube furnace (HTM Reetz Loba). The sample was annealed at 900 °C for 48 hours (5 K/min heating) with subsequent cooling to room temperature at 0.5 K/min, yielding a phase pure compound. For the synthesis route directly from the elements stochiometric amounts thereof were placed in the Nb ampoules without being pressed into a pellet. The samples were treated with the same temperature program as given for the ball milling route, yielding single crystals and minor side phases Sr_4SiP_4 and LiSrP.[17] Due to the educts' and products' sensitivity against air and moisture, all preparations were carried out in an Argon filled glove box (MBraun, <0.1 ppm O_2/H_2O).

Powder X-ray diffraction and Rietveld refinement. Glass capillaries (0.3 mm diameter) were filled with ground samples and sealed under inert conditions. Powder X-ray diffraction was performed on a STOE Stadi P diffractometer (Ge(111) monochromator, Cu $K\alpha_1$ radiation, $\lambda = 1.54056$ Å) with a Dectris MYTHEN 1 K detector in Debye-Scherrer geometry at room temperature. The data was processed using the software package WinXPOW.[18] Rietveld refinement on the obtained data was done using the fullprof software package.[19] The refinement was based on the results of the single crystal analysis.

Single crystal structure determination. A shiny dark red single crystal of $Li_4Sr_2SiP_4$ was obtained in a preliminary reaction of formal composition Li_6SrSiP_4. Powder X-ray analysis of that sample revealed the presence of Li_8SiP_4 and an unknown phase. A crystal of that phase was sealed in a 0.3 mm glass capillary in an argon-filled glove box. The single crystal X-ray diffraction measurement was performed on a Stoe Stadivari diffractometer equipped with a micro source (GENIX, Mo Kα radiation, $\lambda = 0.71073$ Å) and a PILATUS 300 K detector (Dectris) at 150 K. The structure was solved by Direct Methods (SHELXS) and refined by full-matrix least-squares calculations against F^2 (SHELXL).[20] Data reduction and multi-scan absorption correction were carried out with the X-Area (version 1.88, Stoe) and the STOE LANA (version 1.77.1, Stoe) software packages, respectively.[21] Crystallographic data and details of the structure refinement for $Li_4Sr_2SiP_4$ are listed in Table 1. Further details on the structure refinements may be obtained from Fachinformationszentrum Karlsruhe, D-76344 Eggenstein-Leopoldshafen (Germany), by citing the depository number CSD-2312930.

DFT calculations. The computational analysis of $Li_4Sr_2SiP_4$ was performed using the CRYSTAL17 program package and hybrid density functional methods.[22,23] A hybrid exchange-correlation functional after Perdew, Burke, and Ernzerhof (DFT-PBE0) was used.[24] Localized, Gaussian-Type triple ζ-valence + polarization level basis sets were used for Si and P and split valence + polarization level basis sets for Li and Sr. The basis sets were derived from the molecular Karlsruhe basis sets.[25] For the evaluation of the Coulomb and exchange integrals (TOLINTEG), tight tolerance factors of 8, 8, 8, 8, 16 were used for all calculations. The reciprocal space of the structure was sampled with a 5×4×5 Monkhorst-Pack-type *k*-point grid. The starting geometry was taken from experimental data. Both the lattice parameters and atomic positions were fully optimized within the constraints imposed by the space symmetry. Further on the optimized structure was confirmed to be true local minimum by means of harmonic frequency calculation at Γ-point. Electronic band structure and density of states (DOS) were calculated as well as the crystal orbital Hamilton population for all heteroatomic interactions. The Brillouin Zone path of Γ-Z-D-B-Γ-A-E-Z-C_2-Y_2-Γ was provided by the web service *SeeK-path*.[26] Using the results of the frequency calculation, a theoretical Raman spectrum was calculated by utilizing an analytical CPHF/CPKS scheme (coupled perturbed Hartree Fock/Kohn Sham). The full width at half maximum (FWHM) was set to 8 cm^{-1}, the pseudo-Voigt broadening to 50:50 Gaussian:Laurenzian and the laser wavelength to 785 nm. To assign signals in the spectrum to vibrations of the lattice, the software Jmol 14.14.1[27] was used for visualizing the theoretical vibration modes.

Table 1. Crystallographic Data and refinement parameters of the SC-XRD analysis of $Li_4Sr_2SiP_4$.

composition	$Li_4Sr_2SiP_4$
T/K	150
Formula weight/g mol^{-1}	355.0
Crystal size/mm^3	0.05×0.05×0.02
Crystal shape	block
Crystal colour	dark red
Crystal system	monoclinic
Space group	$P2_1/m$ (N°11)
a/Å	7.2919(8)
b/Å	8.3679(6)
c/Å	6.9965(8)
β/°	90.061(9)
Z	2
V/$Å^3$	426.91(7)
ρ_{calc}/g cm^{-3}	2.76
μ/mm^{-1}	13.286
θ range/°	2.793–27.499
Index range (*hkl*)	$-9 \le h \le 9$ $-10 \le k \le 10$ $-9 \le l \le 9$
Reflections collected	4499
Independent Reflections	1043
R_{int}	0.0755
Reflections with $I > 2\sigma(I)$	629
Absorbtion correction	Multi-scan
Data/restraints/parameters	1043/53/0
Goodness of fit on F^2	1.08
R_1, wR_2 (all data)	0.1063, 0.1122
R_1, wR_2 ($I > 2\sigma(I)$)	0.0519, 0.1257
Largest diff. peak/hole/e $Å^{-3}$	1.47/−1.55

Raman spectroscopy. Measurements for powders were carried out at room temperature using the same samples sealed in capillaries used for Powder X-Ray Diffraction. Different spots were measured to ensure reproducibility. Raman spectroscopic measurements for powdered samples were performed using a *inVia* Reflex Raman (Renishaw) system equipped with a CCD Master:Renishaw 266n10 detector (Renishaw) coupled to a Leica DM2700 M microscope (Leica) with 50× magnification and a 785 nm laser with an output power on the sample of 0.1825 mW (sample from ball mill route) and 0.09125 mW (sample directly from elements). The samples were measured for 1 s being repeated 100 times (total measuring time: 100 s). For operating the device and producing the spectra, the software WiRE 5.3 (Renishaw) was used.[28] The installed Rayleigh filter cuts off signals below 110 cm^{-1}.

Results and Discussion

Synthesis and crystal structure of Li_2SrSiP_4. The phase pure microcrystalline product was synthesized from the elements *via* a two steps procedure. At first, stoichiometric amounts of the

elements were ball-milled resulting in a reactive mixture which subsequently was annealed at 900 °C. The product is already formed phase pure at the ball milling step (Figure S1, supporting information). The annealing step, however, increases the crystallinity. Shiny dark red single crystals were obtained from a high temperature reaction of the elements. The gathered single crystal data match the powder X-ray diffraction's results and indicate a phase pure synthesis (Figure 1). $Li_4Sr_2SiP_4$ crystallizes in the monoclinic space group $P2_1/m$ (N°11). Details of the crystal structure data are given in Table 1 and 2 and 3. Rietveld analysis confirms the results (Table S1, supporting information).

As an overview, the crystal structure can be described as a distorted hexagonal close packing of phosphorus atoms in which 50 % of the octahedral voids are occupied by Sr atoms in a layered manner, resulting in CdI_2-like planes of edge sharing octahedra (Figure 2a). Half of the remaining octahedral voids is occupied by Li atoms forming chains of vertex sharing LiP_6 octahedra along the *b*-direction (Figure 2b). The Sr and Li layers lay in the *ab*-plane and alternate. 50 % of all tetrahedral voids are occupied by Li and Si in a 3:1 ratio, resulting in layers of vertex sharing tetrahedra in the *ab*-plane (Figure 3a). With respect to the *c*-direction, the Li containing octahedra and the tetrahedra lay in same plane. Thus, the tetrahedra share faces with the LiP_6 octahedra.

In more detail, the structure of $Li_4Sr_2SiP_4$ is closely related to the $CaAl_2Si_2$ structure type in which similarly 50 % of the octahedral voids of the *hcp* of Si atoms are occupied by Ca and 50 % of the tetrahedral voids are occupied with Al atoms forming layers of edge sharing $AlSi_4$ tetrahedra (Figure 3c) alternating with the Sr layers. In contrast to $CaAl_2Si_2$, tetrahedral voids in the layers in $Li_4Sr_2SiP_4$ are occupied alternatingly by Si and Li atoms, resulting in discrete SiP_4 tetrahedra assuming covalent Si–P bonds (Figure 3a). Thus, the structural motif of discrete SiP_4 tetrahedra is in analogy to Li_8SiP_4 and many other phosphide-based compounds reported by our group in recent years. Overall 25 % of the occupied tetrahedral voids of the *hcp* of P atoms are occupied by Si. These layers of SiP_4 tetrahedra have alternating orientation with respect to the *c*-direction. (Figure 3b). Due to the higher content of cations in $Li_4Sr_2SiP_4$ in contrast to $CaAl_2Si_2$ occupation of half of the remaining

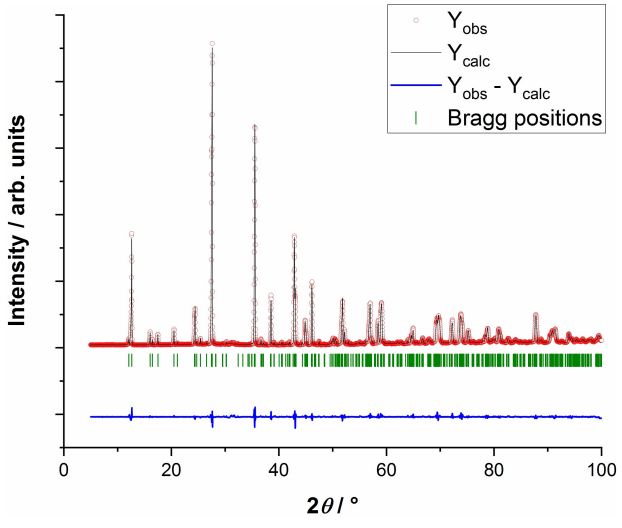

Figure 1. Rietveld refinement on the X-ray powder diffractogram of $Li_4Sr_2SiP_4$ synthesized *via* the ball mill route and subsequent annealing.

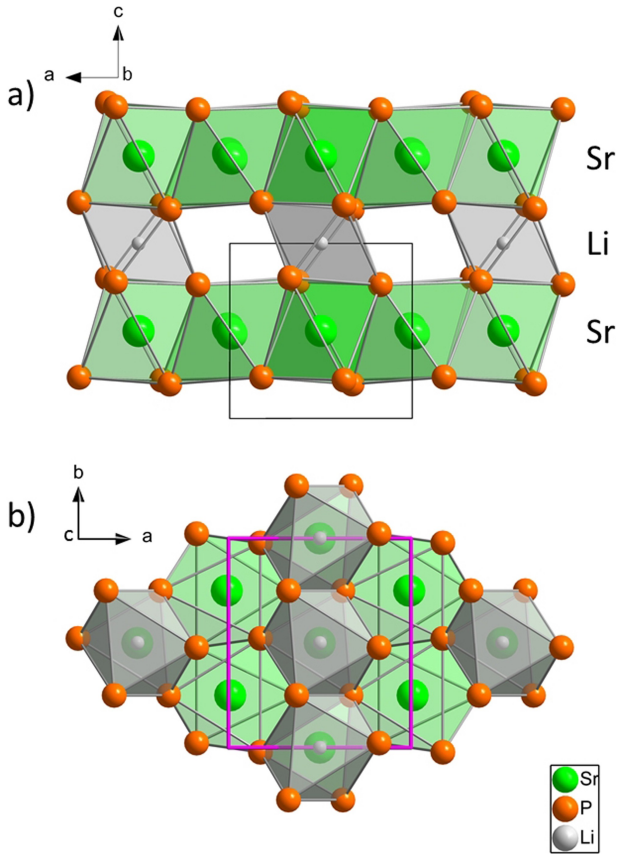

Figure 2. Structure of $Li_4Sr_2SiP_4$ with emphasis on the octahedral void filling with a) and b) viewing along *b* and *c*-direction, respectively. Si and Li atoms occupying tetrahedral voids are omitted. SrP_6 and LiP_6 octahedra are depicted in green and gray color, respectively. The respective central atom is colored alike. P atoms are depicted as orange spheres. a) Layers of SrP_6 octahedra in the *ab*-plane and chains of LiP_6 octahedra along the *b*-direction. The unit cell is given in black. b) The upper Sr layer from a) is removed to not obstruct the view on the chains of vertex sharing LiP_6 octahedra along the *b*-direction. For clarity, the unit cell is given in bold pink.

Table 2. Atom positions and Wyckoff sites in $Li_4Sr_2SiP_4$.

Atom	Wyckoff	Site	x/*a*	y/*b*	z/*c*
Sr1	2d	−1	1/2	0	1/2
Sr2	2e	m	0.0094(2)	1/4	0.5149(3)
P1	4f	1	0.1748(4)	0.9781(3)	*0.7643(4)*
P2	2e	m	0.6712(5)	1/4	0.8035(7)
P3	2e	m	0.3732(6)	1/4	0.2194(6)
Si1	2e	m	0.6838(6)	1/4	0.1321(7)
Li1	4f	1	0.848(3)	0.989(2)	0.884(3)
Li2	2e	m	0.322(4)	1/4	0.874(5)
Li3	2b	−1	1/2	0	0

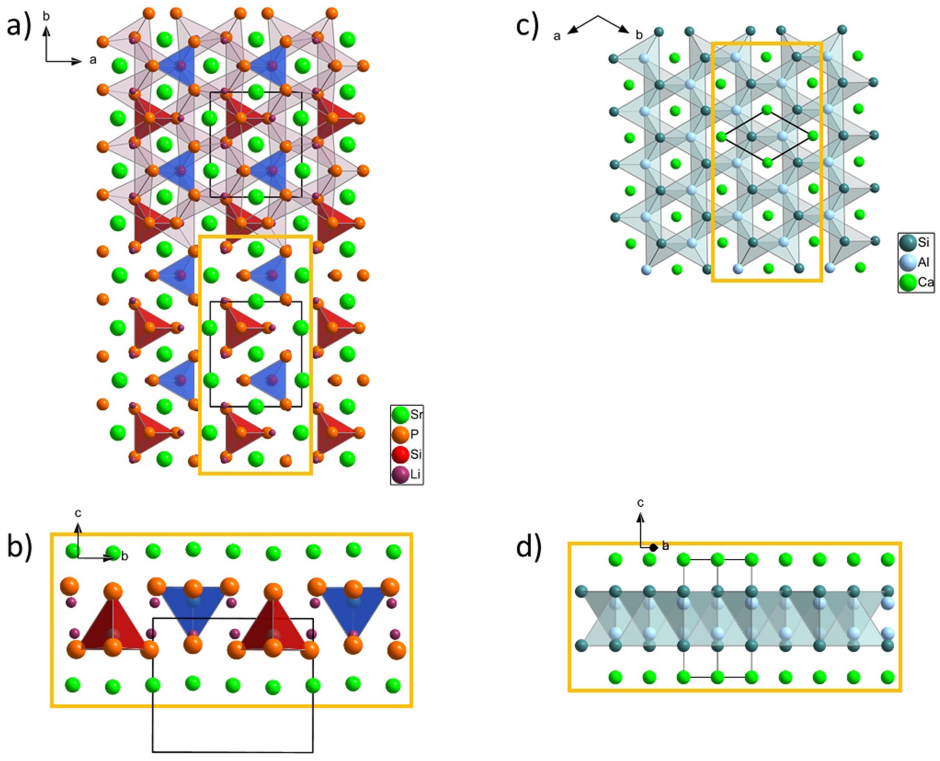

Figure 3. Structure of $Li_4Sr_2SiP_4$ and $CaAl_2Si_2$ with emphasis on the tetrahedral void filling. a) and c) show the same structural motif perpendicular to the layers of filled tetrahedral voids in $Li_4Sr_2SiP_4$ and $CaAl_2Si_2$, respectively, as well as the monoclinic and trigonal unit cells in black. SiP_4 tetrahedra are colored red if the trigonal tetrahedron face is located in negative *c*-direction compared to the remaining corner. Tetrahedra are shown in blue if the face points upwards; LiP_4 tetrahedra are colored in faint violet and are omitted in the lower part of Figure 3a). Sr (and Ca in $CaAl_2Si_2$, respectively) is depicted as green spheres. Tetrahedral Li is depicted as violet spheres, Li atoms in octahedral voids are omitted. P is depicted as orange spheres. $AlSi_4$ tetrahedra are depicted in gray. Si is depicted as petrol spheres in $CaAl_2Si_2$. b) and d) show the tetrahedra in layer direction. b) corresponds to the marked area in a) and d) to the one in c).

Table 3. Displacement parameters in $Li_4Sr_2SiP_4$. For tetrahedral Li (Li1 and Li2) only isotropic displacement parameters are given.

Atom	U11	U22	U33	U12	U13	U23
Sr1	0.0089(6)	0.0075(6)	0.0103(7)	0.0004(6)	0.0001(5)	0.0004(6)
Sr2	0.0115(7)	0.0101(7)	0.0137(8)	0.0000	−0.0012(6)	0.0000
P1	0.010(1)	0.009(1)	0.010(1)	0.000(1)	−0.000(1)	0.002(1)
P2	0.010(2)	0.009(2)	0.014(2)	0.0000	−0.002(2)	0.0000
P3	0.012(2)	0.007(2)	0.012(2)	0.0000	0.001(2)	0.0000
Si1	0.012(2)	0.005(2)	0.013(2)	0.0000	−0.000(2)	0.0000
Li1	0.016(4)					
Li2	0.019(6)					
Li3	0.005(9)	0.006(9)	0.01(1)	0.00(1)	0.002(9)	0.00(1)

octahedral voids by Li occurs. As a result, chains of face sharing octahedra occupied alternatingly by Sr and Li along the *c*-direction emerge. The LiP_6 octahedra lay in the layers of tetrahedra and share faces with them, building chains *via* shared vertices themselves (Figure 2b).

Besides the P atom packing type in $Li_4Sr_2SiP_4$ there are also significant differences to the *ccp* in Li_8SiP_4 regarding interatomic distances. P–P distances in the *hcp* of P atoms in $Li_4Sr_2SiP_4$ range from 3.631(6) Å to 3.817(4) Å and are thus significantly shorter than in Li_8SiP_4 with all P–P distances being longer than 4.18 Å. In $Li_4Sr_2SiP_4$ the Si–P distances are in the range of 2.287(4) Å to 2.345(6) Å and thus slightly longer than the Si–P distances in Li_8SiP_4 that range from 2.2420(2) Å to 2.2979(1) Å. However, they are still in the typical range for covalent Si–P bonds as also later on confirmed by DFT calculations. Both interatomic distance trends can be explained by the presence of Sr^{2+} cations in the structure. Aside from apparently changing the type of closest packing, the presence of the alkaline-earth metal in contrast to Li ions leads to a denser packing of P atoms through stronger ionic interactions.

The $Li_4Sr_2SiP_4$ structure furthermore can be described as 2×2×1 superstructure of the $CaAl_2Si_2$ structure type (Figure 4).

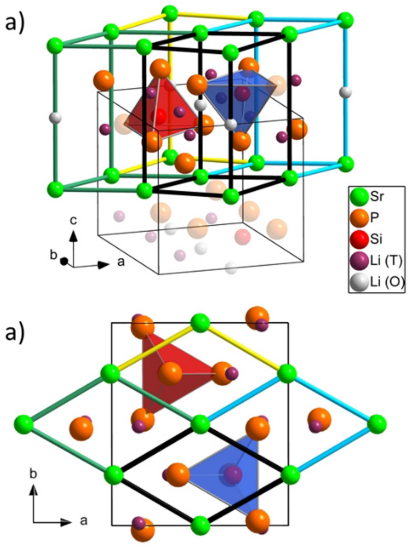

Figure 4. The $Li_4Sr_2SiP_4$ structure as superstructure of the $CaAl_2Si_2$ structure type. Every second octahedral void that is not occupied by Sr (green spheres) is occupied by Li (gray spheres opposed to Li atoms depicted as violet spheres in tetrahedral voids). There are two isolated SiP_4 tetrahedra (red if trigonal tetrahedron base is located in negative *c*-direction compared to the remaining tetrahedron edge = "up", blue if oriented the other way = "down") in four $CaAl_2Si_2$ type units (highlighted in black, green, blue and yellow) arranged alternatingly. P is depicted as orange spheres. The rest of the monoclinic unit cell (thin black cell edges) of the $Li_4Sr_2SiP_4$ structure is rendered transparent for clarity. b) shows the same part of the structure as a), but along *c*-direction.

In $CaAl_2Si_2$ 50% of all octahedral and tetrahedral voids are occupied by Ca and Al, respectively. Accordingly, the sum formula can be written as $Ca\square^{O}Al_2\square^{T}{}_2Si_2$, where O and T denote octahedral and tetrahedral positions, and □ a vacant site. In $Li_4Sr_2SiP_4$, too, 50% of all tetrahedral voids are filled. Out of the filled tetrahedral voids, 25% are occupied by Si and 75% by Li. With respect to all existing tetrahedral voids, this amounts to 12.5% and 37.5% of tetrahedral void occupation by Si and Li, respectively. In contrast to $CaAl_2Si_2$, 75% of all octahedral voids are filled in $Li_4Sr_2SiP_4$. Out of the filled octahedral voids in $Li_4Sr_2SiP_4$, two thirds are occupied by Sr and one third by Li. With respect to all existing octahedral voids, this amounts to a filling of 50% and 25% of all octahedral voids by Sr and Li, respectively. While Sr occupies the sites occupied by Ca in $CaAl_2Si_2$, Li occupies a site, that is vacant in $CaAl_2Si_2$. The sum formula of $Li_4Sr_2SiP_4$ therefore can be written as $Sr_2\square^{O}Li^{O}Si^{T}Li^{T}{}_3\square^{T}{}_4P_4$, as compared to $Ca_2\square^{O}{}_2Al_4\square^{T}{}_4Si_4$ (= 2 x $Ca\square^{O}Al_2\square^{T}{}_2Si_2$). So far, this expression states that two $CaAl_2Si_2$-like units are needed to represent the $Li_4Sr_2SiP_4$ structure. Yet, to fully describe the relationship between the structures, the orientation of the SiP_4 tetrahedra has to be considered. Since they alternate in orientation with respect to the *c*-axis, two Si atoms have to be present in the sum formula. If a tetrahedron is considered to be orientated "up" - its triangular base points in negative *c*-direction and the remaining corner in positive *c*-direction - one can write $Sr_4\square^{O}{}_2Li^{O}{}_2Si^{up}Si^{down}Li^{T}{}_6\square^{T}{}_8P_8$, which is a sum formula analogue to $Ca_4\square^{O}{}_4Al_8\square^{T}{}_8Si_8$ (= 4 x $Ca\square^{O}Al_2\square^{T}{}_2Si_2$). If all remaining octahedral voids were occupied, the Li_3LaSb_2 structure type would result. It can be understood as a completely filled variant of the $CaAl_2Si_2$ structure type in terms of octahedral voids. $Li_4Sr_2SiP_4$ thus links those two structure types in terms of occupation of octahedral voids, despite belonging to a different crystal system. It can either be seen as a partially filled variant of the $CaAl_2Si_2$ structure type or as a defect variant of the Li_3LaSb_2 structure type.

This arrangement of atoms can be achieved by symmetry reduction[29] of the trigonal $CaAl_2Si_2$ structure type (space group $P\bar{3}m1$, N° 164) *via* *C*2/*m* (N° 12) and *P*2/*m* (N° 10) to $P2_1/m$ (N° 11). The corresponding Bärnighausen tree is depicted in Figure 5. Since *P*2/*m* is not a direct subgroup of $P\bar{3}m1$, a symmetry reduction to *C*2/*m* is required. The 4*i* positions in *P*2/*m* split into 2 *m* and 2*e* positions each, allowing the tetrahedral voids to be occupied by different elements. Further splitting of the 2 *m* position in two 2*e* positions in $P2_1/m$ creates three possible tetrahedral positions (4*f* and 2×2*e*) which allows for occupation of tetrahedral voids by different elements in a 3:1 ratio (Li:Si) as observed in $Li_4Sr_2SiP_4$, resulting ultimately in the distortion of the *hcp*, which is allowed for the same reason. The additional 2*b* position occupied only in $Li_4Sr_2SiP_4$ corresponds to the octahedral Li. Note, that the refined atomic coordinates, due to distortion, deviate slightly from the coordinates obtained by pure symmetry reduction. The standardization of all atomic coordinates was accomplished *via* the STRUCTURE TIDY implementation of the PLATON package[30] available on the bilbao crystallographic server.[31]

The trigonal cell of $CaAl_2Si_2$ and its analogue in the $Li_4Sr_2SiP_4$ structure are also similar in size. In $CaAl_2Si_2$ the Ca–Ca distances are equal to the *a* and *c*-parameters of the unit cell (4.1300 Å and 7.1450 Å, respectively). The corresponding Sr–Sr distances in $Li_4Sr_2SiP_4$, where the arrangement of the Sr atoms, too, is slightly distorted, range from 4.145(1) Å to 4.264(1) Å and from 6.996(3) Å to 6.9965(8) Å, respectively. The Sr–Sr-Sr angle corresponding to the ideal 120° angle in the trigonal cell is 120.233(7)°. While the structures belong to different crystal systems, the structures themselves and the motif within are strongly related.

Electronic structure of $Li_4Sr_2SiP_4$. The experimental structure of $Li_4Sr_2SiP_4$ was used as input geometry for crystal structure optimization. Since the maximum deviation between experimental and calculated lattice parameters is only 0.46% (Table S2, supporting information) and the compound was found to be a true minimum on the potential energy surface due to the absence of imaginary frequencies, band structure, density of states (DOS) and crystal orbital Hamilton population (COHP) were calculated. Both plots can be found in Figure 6 and 7, respectively.

The compound has an indirect band gap of 2.73 eV with a transition from Γ to Y_2. In general, the bands show a moderate dispersion in valence and conduction bands. The density of states shows mostly P atom states below the Fermi-Level, especially between −0.5 and 0 eV, where it is the sole contributor. For lower energies minor contributions of Li, Sr and

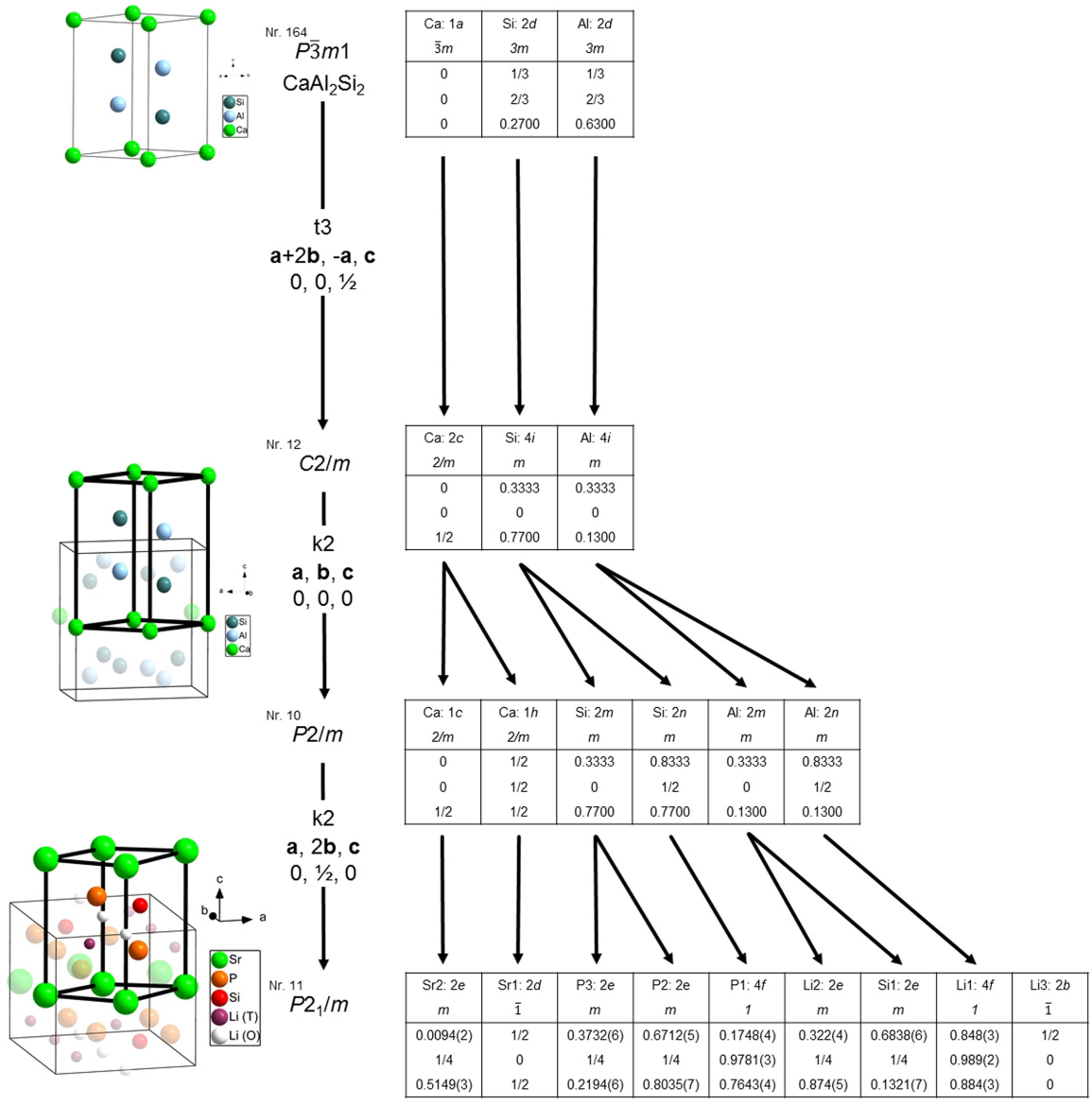

Ca: 1*a*	Si: 2*d*	Al: 2*d*
$\bar{3}m$	3*m*	3*m*
0	1/3	1/3
0	2/3	2/3
0	0.2700	0.6300

Ca: 2*c*	Si: 4*i*	Al: 4*i*
2/*m*	*m*	*m*
0	0.3333	0.3333
0	0	0
1/2	0.7700	0.1300

Ca: 1*c*	Ca: 1*h*	Si: 2*m*	Si: 2*n*	Al: 2*m*	Al: 2*n*
2/*m*	2/*m*	*m*	*m*	*m*	*m*
0	1/2	0.3333	0.8333	0.3333	0.8333
0	1/2	0	1/2	0	1/2
1/2	1/2	0.7700	0.7700	0.1300	0.1300

Sr2: 2*e*	Sr1: 2*d*	P3: 2*e*	P2: 2*e*	P1: 4*f*	Li2: 2*e*	Si1: 2*e*	Li1: 4*f*	Li3: 2*b*
m	$\bar{1}$	*m*	*m*	1	*m*	*m*	1	$\bar{1}$
0.0094(2)	1/2	0.3732(6)	0.6712(5)	0.1748(4)	0.322(4)	0.6838(6)	0.848(3)	1/2
1/4	0	1/4	1/4	0.9781(3)	1/4	1/4	0.989(2)	0
0.5149(3)	1/2	0.2194(6)	0.8035(7)	0.7643(4)	0.874(5)	0.1321(7)	0.884(3)	0

Figure 5. Bärnighausen tree depicting the symmetry reduction of the $CaAl_2Si_2$ (space group $P\bar{3}m1$, N° 164) structure to the $Li_4Sr_2SiP_4$ structure (space group $P2_1/m$, N° 11). The unit resembling the $CaAl_2Si_2$ structure type is highlighted in all structures with reduced symmetry.

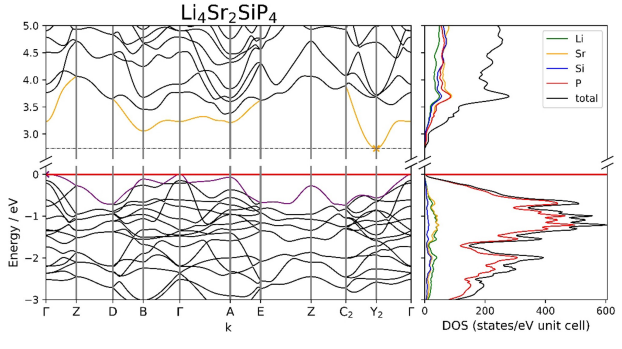

Figure 6. Band structure and atom projected DOS of $Li_4Sr_2SiP_4$ with an indirect band gap of 2.73 eV.

Si atoms can be found. For the conduction bands all atoms contribute almost equal amounts of states.

Although the DOS shows many P atom states just below the Fermi-Level, P atoms are not involved in interatomic interactions just below the Fermi-Level in the COHP. Thus, these states can be assigned to P atom lone pairs. Only some Li–P interactions can be found for lower valence bands. In contrast the conduction bands show strong Si–P anti-bonding interactions as well as minor Li–Si anti-bonding and Li–P bonding interactions. The Former are of particular interest since they are the only ones present between 2.73 and 3 eV where only the first conduction band at the conduction band minimum (CBM) is present in the band structure. Since this band is pulled down at Y_2 compared to the other k-points this leads to the

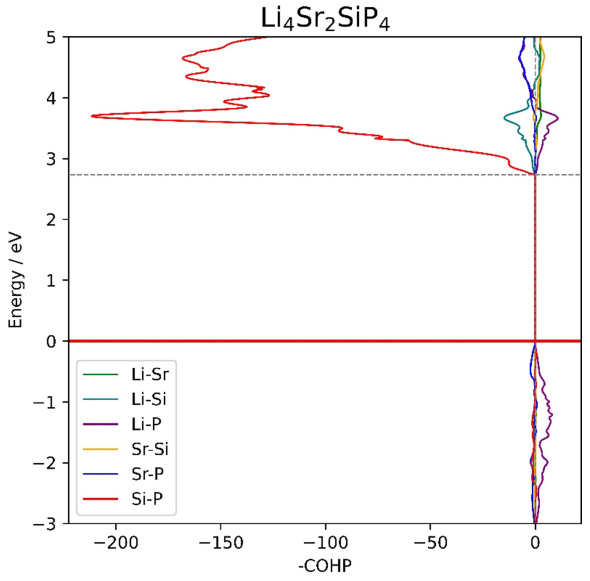

Figure 7. COHP of all heteroatomic interactions of $Li_4Sr_2SiP_4$. Bonding and anti-bonding contributions are plotted to the right and left side, respectively.

assumption that low lying, unoccupied states of Si–P anti-bonding interactions are responsible for the indirect band gap.

For a better understanding of the electronic structure of $Li_4Sr_2SiP_4$, a Mullikan analysis was conducted. Interatomic distances and overlap populations can be found in Table S3 (supporting information) for the six closest interactions of each atom in the unit cell. The highest overlap can be found for Si–P interactions with values between 0.305 and 0.251, confirming bonds within the tetrahedra. For Li and Sr only minor interactions with themselves and each other can be found contrary to their interaction with Si and P. Although the overlap population values are still small, they could be attributed to weak ionic interactions between positively charged Li^+ and Sr^{2+} and negatively charged SiP_4^{8-} tetrahedra.

Raman Spectroscopy. The Raman spectra of powdered $Li_4Sr_2SiP_4$ obtained by the two synthetic methods are shown in Figure 8. The Raman spectra are in excellent agreement with the calculated one. Since the calculations assume a structure at 0 K the intensities differ from room temperature measurements. A correction factor of 0.96 has been applied to compensate for the calculation's overestimation of wavenumbers at high wavenumbers. Nevertheless, a slight disagreement between theoretical and measured values is to be expected and can be seen here as well. The eight most intense peaks can be attributed to different stretching and deformation modes of the SiP_4 tetrahedra (Table S4, supporting information), which are always accompanied by lattice vibrations of Li and Sr normal modes. Due to the distortion assignment of ideal tetrahedral modes is not possible, but the normal modes present can still be categorized and classified by visualization.

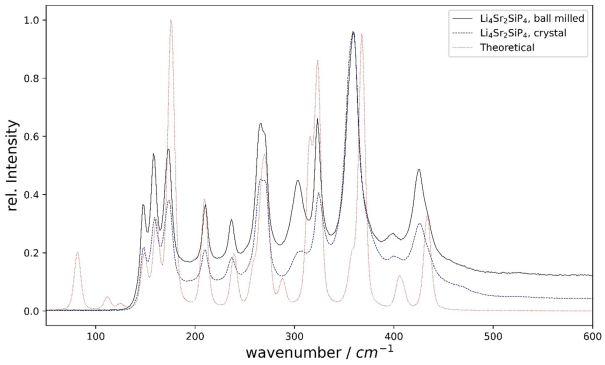

Figure 8. Raman spectra of a sample obtained after ball milling of the elements and subsequent annealing and of a sample yielded by direct reaction of the elements shown as black and dashed blue, respectively. The calculated Raman spectra is shown as dotted redline.

Conclusions

The novel phase $Li_4Sr_2SiP_4$ could be synthesized phase pure *via* ball milling and subsequent annealing. Single crystals of the title compound were obtained by direct reaction of the elements at elevated temperatures. Preliminary reactions showed that $Li_4Sr_2SiP_4$ has no phase width in terms of $Li_{8-2x}Sr_xSiP_4$, since a sample of formal composition Li_6SrSiP_4 resulted in the two phases Li_8SiP_4 and $Li_4Sr_2SiP_4$, which in sum match exactly the doubled formal composition. Single crystal analysis shows that $Li_4Sr_2SiP_4$ crystallizes in a new structure type that represents a link between the $CaAl_2Si_2$ structure type and the Li_3LaSb_2 structure type in terms of octahedral void occupation. The compound's colour matches the calculated band gap considering the general overestimation of band gaps by the used functionals.[32] DFT calculations on $Li_4Sr_2SiP_4$ proved to be trustworthy: the calculated lattice parameters as well as the theoretical Raman spectrum are in excellent agreement with the measured values.

Supporting Information

Additional powder X-ray diffraction data, further information on the Rietveld refinement, calculated interatomic distances and overlap population, comparison of experimental and optimized cell parameters, listed peaks of the Raman spectra.

Note added in proof

During the revision of this article, a paper on the synthesis and structure of the title compound found independently using a different synthesis method has been published as accepted article (*Chem. Eur. J.*2023, e20230369).

Notes

The authors declare no competing financial interest.

Acknowledgements

The authors are grateful to the Bavarian Ministry of Economic Affairs, Regional Development, and Energy for funding their research in the project "Industrialisierbarkeit von Festkörperelektrolytzellen". D.D thanks the Deutsche Forschungsgemeinschaft (DFG, German Research Foundation, project number 245845833) within the International Research Training Group IRTG 2022 (ATUMS) for financial support. Open Access funding enabled and organized by Projekt DEAL.

Conflict of Interest

The authors declare no conflict of interest.

Data Availability Statement

The data that support the findings of this study are available in the supplementary material of this article.

Keywords: Pnictides · Zintl Phase · Lithium

[1] a) J. Janek, W. G. Zeier, *Nat. Energy* **2016**, *1*, 1–4; b) A. L. Robinson, J. Janek, *MRS Bull.* **2014**, *39*, 1046–1047; c) S. Ohno, A. Banik, G. F. Dewald, M. A. Kraft, T. Krauskopf, N. Minafra, P. Till, M. Weiss, W. G. Zeier, *Prog. Energy* **2020**, *2*, 22001.
[2] L. Toffoletti, H. Kirchhain, J. Landesfeind, W. Klein, L. van Wüllen, H. A. Gasteiger, T. F. Fässler, *Chem. Eur. J.* **2016**, *22*, 17635–17645.
[3] T. M. F. Restle, C. Sedlmeier, H. Kirchhain, W. Klein, G. Raudaschl-Sieber, V. L. Deringer, L. van Wüllen, H. A. Gasteiger, T. F. Fässler, *Angew. Chem. Int. Ed. Engl.* **2020**, *59*, 5665–5674.
[4] a) S. Strangmüller, H. Eickhoff, D. Müller, W. Klein, G. Raudaschl-Sieber, H. Kirchhain, C. Sedlmeier, V. Baran, A. Senyshyn, V. L. Deringer, L. van Wüllen, H. A. Gasteiger, T. F. Fässler, *J. Am. Chem. Soc.* **2019**, *141*, 14200–14209; b) S. Strangmüller, H. Eickhoff, G. Raudaschl-Sieber, H. Kirchhain, C. Sedlmeier, L. van Wüllen, H. A. Gasteiger, T. F. Fässler, *Chem. Mater.* **2020**, *32*, 6925–6934.
[5] B. Eisenmann, H. Jordan, H. Schäfer, *Mater. Res. Bull.* **1982**, *17*, 95–99.
[6] B. Eisenmann, M. Somer, *Zeitschrift für Naturforschung B* **1984**, *39*, 736–738.
[7] X. Zhang, T. Yu, C. Li, S. Wang, X. Tao, *Z. Anorg. Allg. Chem.* **2015**, *641*, 1545–1549.
[8] A. Haffner, T. Bräuniger, D. Johrendt, *Angew. Chem. Int. Ed. Engl.* **2016**, *55*, 13585–13588.
[9] A. Haffner, A.-K. Hatz, O. E. O. Zeman, C. Hoch, B. V. Lotsch, D. Johrendt, *Angew. Chem. Int. Ed. Engl.* **2021**, *60*, 13641–13646.
[10] A. Haffner, V. Weippert, D. Johrendt, *Z. Anorg. Allg. Chem.* **2021**, *647*, 326–330.
[11] B. Eisenmann, H. Jordan, H. Schäfer, *Zeitschrift für Naturforschung B* **1984**, *39*, 864–867.
[12] J. Mark, J.-A. Dolyniuk, N. Tran, K. Kovnir, *Z. Anorg. Allg. Chem.* **2019**, *645*, 242–247.
[13] A. Haffner, V. Weippert, D. Johrendt, *Z. Anorg. Allg. Chem.* **2020**, *646*, 120–124.
[14] G. Akopov, J. Mark, G. Viswanathan, S. J. Lee, B. C. McBride, J. Won, F. A. Perras, A. L. Paterson, B. Yuan, S. Sen, A. N. Adeyemi, F. Zhang, C.-Z. Wang, K.-M. Ho, G. J. Miller, K. Kovnir, *Dalton transactions (Cambridge, England : 2003)* **2021**, *50*, 6463–6476.
[15] E. I. Gladyshevskii, P. I. Krypyakevych, O. I. Bodak, *Ukr. Phys. J.* **1967**, *12*, 447–452.
[16] I. Grund, H.-U. Schuster, P. Müller, *Z. Anorg. Allg. Chem.* **1984**, *515*, 151–158.
[17] Y. Dong, F. J. DiSalvo, *J. Solid State Chem.* **2007**, *180*, 432–439.
[18] *WinXPOW*, *version 3.0.2.1*, STOE & Cie GmbH, Darmstadt, Germany, **2011**.
[19] Juan Rodriguez-Carvajal, *FullProf*, *version 3.00*, Institut Laue-Langevin, **2015**.
[20] G. M. Sheldrick, *Acta Crystallogr. Sect. C* **2015**, *71*, 3–8.
[21] a) *X-Area*, *version 1.90*, STOE & Cie GmbH, Darmstadt, Germany, **2020**; b) *LANA*, *version 1.77.1*, STOE & Cie GmbH, Darmstadt, Germany, **2020**.
[22] R. Dovesi, V. R. Saunders, C. Roetti, R. Orlando, C. M. Zicovich-Wilson, F. Pascale, B. Civalleri, K. Doll, N. M. Harrison, I. J. Bush, P. D'Arco, M. Llunell, M. Causà, Y. Noël, L. Maschio, A. Erba, M. Rerat, S. Casassa, CRYSTAL 17 User's Manual, University of Torino, Torino, Italy, **2017**.
[23] R. Dovesi, A. Erba, R. Orlando, C. M. Zicovich-Wilson, B. Civalleri, L. Maschio, M. Rérat, S. Casassa, J. Baima, S. Salustro, B. Kirtman, *Wiley Interdiscip. Rev.: Comput. Mol. Sci.* **2018**, *8*, e1360.
[24] J. P. Perdew, W. Yang, K. Burke, Z. Yang, E. K. U. Gross, M. Scheffler, G. E. Scuseria, T. M. Henderson, I. Y. Zhang, A. Ruzsinszky, H. Peng, J. Sun, E. Trushin, A. Görling, *Proc. Natl. Acad. Sci. USA* **2017**, *114*, 2801–2806.
[25] a) A. J. Karttunen, T. F. Fässler, M. Linnolahti, T. A. Pakkanen, *Inorg. Chem.* **2011**, *50*, 1733–1742; b) T. M. F. Restle, J. V. Dums, G. Raudaschl-Sieber, T. F. Fässler, *Chem. Eur. J.* **2020**, *26*, 6812–6819; c) G. Sansone, L. Maschio, D. Usvyat, M. Schütz, A. Karttunen, *J. Phys. Chem. Lett.* **2016**, *7*, 131–136; d) B. Scheibe, C. Pietzonka, O. Mustonen, M. Karppinen, A. J. Karttunen, M. Atanasov, F. Neese, M. Conrad, F. Kraus, *Angew. Chem. Int. Ed. Engl.* **2018**, *57*, 2914–2918.
[26] Y. Hinuma, G. Pizzi, Y. Kumagai, F. Oba, I. Tanaka, *Comput. Mater. Sci.* **2017**, *128*, 140–184.
[27] *Jmol. An open-source Java viewer for chemical structures in 3D*, http://www.jmol.org.
[28] Renishaw, *WiRE. inVia Reflex Raman*, Pliezhausen, Germany.
[29] U. Müller in *Symmetriebeziehungen zwischen Kristallstrukturen* (Ed.: U. Müller), Springer Berlin Heidelberg, Berlin, Heidelberg, **2023**, pp. 159–163.
[30] A. L. Spek, *J. Appl. Crystallogr.* **2003**, *1*, 7–13.
[31] "Bilbao Crystallographic Server", can be found under http://www.cryst.ehu.es.
[32] B. Civalleri, D. Presti, R. Dovesi, A. Savin in *Chemical Modelling* (Ed.: M. Springborg), Royal Society of Chemistry, Cambridge, **2012**, pp. 168–185.

Manuscript received: December 12, 2023
Revised manuscript received: December 28, 2023
Accepted manuscript online: December 29, 2023

